Methylene Blue Removal of Fixed-Bed Column Reactor with Pumice and nZVI-Pumice: Experimental and Modeling Study

Mesut GENİŞOĞLU[1] , **Ayşegül Yağmur GÖREN[2]** , **Esin BALCI[3]** , **Yaşar Kemal RECEPOĞLU[4]** , **Hatice Eser ÖKTEN[*5]**

[1,2,3,5]İzmir Institute of Technology, Faculty of Engineering, Department of Environmental Engineering, 35430, İzmir, Turkey
[4]İzmir Institute of Technology, Faculty of Engineering, Department of Chemical Engineering, 35430, İzmir, Turkey

Abstract: Nano zero-valent iron (nZVI) emerges as a low cost and eco-friendly adsorbent to treat textile wastewater, which is rich in dye content. However nZVI particles can easily agglomerate in aqueous environment due to electrostatic interaction, decreasing their treatment efficiency. Therefore pumice, a low-cost and naturally found porous material with lower specific surface area ($2m^2/gr$), can be used as support material to reduce agglomeration of nZVI. Treatment efficiencies of pumice/nZVI packing (10:0 and 9:1 (w/w)) in column reactor for specified initial methylene blue concentrations (25, 50, 75 and 100 mg/L) were investigated in this study. Adsorption capacities of the adsorbents were calculated as 2.8 and 4.2 mg/g-adsorbent, respectively at 100 mg/L initial methylene blue concentration. Mixed bed column performed significantly better than its pumice-only counterpart for low initial concentrations. Thomas adsorption model was applied to experimental results with a moderate to high predictive power.

Pomza ve nSDD-Pomza ile Sabit Yataklı Kolon Reaktörde Metilen Mavisi Giderimi: Deneysel ve Modelleme Çalışması

Özet: Nano sıfır değerlikli demir (nSDD) yüksek renk konsantrasyonlarına sahip tekstil atıksularının arıtımında ekonomik ve çevre dostu bir adsorban olarak ortaya çıkmaktadır. Ancak nSDD partikülleri sulu çözeltilerde elektrostatik etkileşimler sebebiyle kolayca topaklaşmakta ve bu da arıtma veriminin düşmesine neden olmaktadır. Dolayısıyla düşük maliyetli, doğal poröz yapıda ve ortalama $2m^2/gr$ spesifik yüzey alanına sahip pomza, nSDD topaklaşmasını önleyici bir malzeme olarak kullanılabilir. Bu çalışmada sadece pomza ve pomza-nSDD (ağırlıkça 9:1) karışımının kullanıldığı kolon reaktörde 25, 50, 75 ve 100 mg/L metilen mavisi konsantrasyonları için arıtma verimleri incelenmiştir. Pomzanın ve pomza-nSDD karışımının 100 mg/L metilen mavisi deneyindeki toplam kapasiteleri sırasıyla 2,8 ve 4,2 mg/g-adsorban olarak bulunmuştur. Özellikle düşük konsantrasyonlarda, pomza-nSDD karışımının arıtma performansını önemli ölçüde arttırdığı görülmüştür. Thomas modeli deneysel verilere uygulanmış ve modelin öngörü gücünün düşük konsantrasyonda yüksekken, yüksek konsantrasyonlarda ortalama olduğu kanısına varılmıştır.

,

1. Introduction

Textile industry is known as a sector of high water demand, which is estimated as 80 – 100 m³ per ton of finished textile, hence having the biggest impact on environment through primary water consumption and wastewater production. Therefore, environmentally sustainable development in textile industry is necessary for closing of water cycle [1]. However, synthetic organic dyes are extensively used in textile production process [2] and large volumes of wastewaters with high concentration of dyes are generated. Direct release of these colored wastewaters without meeting required discharge limits would have adverse effects on environment and human health [3].

Methylene blue (MB) is one of the most important organic pollutants used in textile, food, dyeing, printing, cosmetic, plastics, paper and manufacturing industries [4]. MB is non-degradable in nature and it is significantly toxic [5,6]. On account of these properties, MB adversely affects the environment and human beings [7]. It may cause irritation, gastritis, diarrhea, cyanosis, tissue necrosis, nausea, jaundice and vomiting in humans [8,9].

There are several conventional treatment methods for textile wastewater including oxidation [10], electrochemical techniques [11], coagulation [12], ultrafiltration [13], adsorption [14] and nanomaterials [15]. However, some of these methods have disadvantages such as high costs, non-applicability in large scale, complexity of operation and production of toxic sludge [3,16]. Among them, adsorption is the most often used one, providing relatively less waste production, regeneration of materials at the end of the process, high efficiency, ease of operation, nonproduction of toxic sludge, and economical feasibility associated with low adsorbent cost [17–20].

Textile wastewater treatment costs were reported to be in the range of 1.37-2.01 $/m³ by using four different combinations of nanofiltration, ultrafiltration and microfiltration membranes [21]. Operation cost of COD removal from textile wastewater using electrocoagulation was in the range of 0.1 - 0.3 $/m³ [22], considering only COD and turbidity removal. Chemical costs for alum coagulation and Fenton oxidation were 1.30 and 2.50 $/m³, whereas color removal efficiencies were 34% and 24%, respectively [23]. Chemical cost of GAC adsorption was determined as 1.50 $/m³ with a color removal efficiency of 88%. Considering highly colored textile effluent volumes per unit production, development of a cheap and effective treatment system is essential.

Due to its superior properties such as technical feasibility, non-toxicity, low cost, high reactive surface area and subsequently shorter treatment times, nZVI can be considered as a promising alternative for adsorbent material in dye removal [24]. However, in fixed bed operations, limitations emerge as nZVI particles agglomerate. Subsequently, hydraulic conductivity and surface area of nZVI particles decrease, compromising treatment efficiency [24-27]. In order to overcome these limitations and increase stability, support materials such as anionic polymer, chitosan, activated carbon, and starches are recommended as support material [26,28-31]. Moreover, due to their porous structure, pumice, bentonite and kaolinite have been preferred as support material to improve dispersibility of nZVI particles [26,28]. Among these porous materials, pumice is a volcanic rock with high surface area. Also, it is used as an effective, low-cost adsorbent to remove dye and heavy metals from water sources [31-34]. In the current literature, only a few studies focused on removal of heavy metals from water sources using pumice as support material for nZVI. However, no studies have been found about pumice usage as support material for nZVI to remove dye from wastewater.

In this work, adsorption performances of only pumice and mixed-bed nZVI-pumice by chromatographic separation were investigated for dye removal from model dye solutions by changing initial concentration. Also, the mixed-bed column behavior was interpreted by applying a dynamic model - Thomas model [35] to validate experimental data with theoretical ones obtained from breakthrough curves.

2. Materials and Methods

2.1. Materials

Commercial air-stabilized nZVI samples (NANOFER STAR; %60-80 nZVI-%20-40 iron oxides) were supplied from NanoIRON, s.r.o., CZ. The pumice used in this study originated from Isparta province. Pumice samples were supplied from Pumice Research and Application Center in Süleyman Demirel University, Isparta. Pumice samples were grounded and separated into fractions below 63 microns after grinding. Also, pumice and nZVI particles were mixed with grinding. Methylene blue ($C_{16}H_{18}N_3SCl$) was purchased from Fluka AG, reagent grade. Model dye solutions were prepared using deionized water. MB stock solution was prepared (1000 ppm) and serial dilutions were made to obtain MB concentrations of 25, 50, 75, and 100 ppm. Concentrations of MB were measured at λ_{max} of 664 nm by UV-visible spectrophotometer (Shimadzu, UV-2600).

2.1. Adsorption tests and Thomas model

Adsorption studies were conducted in a glass column at continuous flow mode (Figure 1). Column was packed with different adsorbents (pumice and pumice-nZVI mixed bed). Methylene blue solutions were fed from the top of the column and samples were collected at 3 min intervals from the bottom. In all experiments, room temperature and pH of solutions (7.0) were kept constant. Adsorption capacity of selected adsorbent was determined by using equation (1):

$$qe = \frac{C_0 - C_f}{m} \times V \qquad (1)$$

where qe is the adsorption capacity of the adsorbent (mg MB/g adsorbent), C_0 and C_f are initial MB concentration and effluent MB concentration (mg/L), respectively, V is the volume of solution (L), and m is the amount of adsorbent (g).
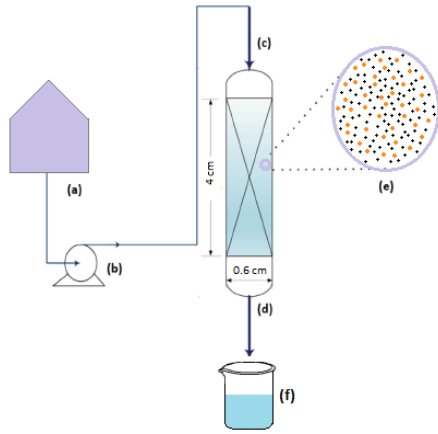
Figure 1. Schematic representation of the experimental setup for mixed-bed glass column experiments: (a) feed, (b) peristaltic pump, (c) feed inlet, (d) glass column, (e) mixed-bed, (f) collected effluent.

Removal efficiency (Re) of MB was determined using equation (2):

$$Re\ (\%) = \frac{C_0 - C_f}{C_0} \times 100 \qquad (2)$$

Experimental data were used to fit Thomas adsorption model for estimating the theoretical condition. Thomas adsorption model calculates the maximum amount of sorbed material and rate constant of the adsorption column. Thomas model assumes kinetics of adsorption–desorption of Langmuir without dispersion. However, the main restriction of Thomas model is that adsorption is controlled by mass transfer at the interface and not limited by chemical reaction [36]. Equation of Thomas model can be described as:

$$\frac{C}{C_0} = \frac{1}{1 + exp(K_T(q_o m - C_0 \vartheta)/Q)} \qquad (3)$$

where K_T is the constant (mL/(min mg)) and ϑ is the solution volume percolated through column.

3. Results and Discussion

3.1. XRD analysis of adsorbents

XRD spectrums for pumice, nZVI and pumice/nZVI mix are shown in Figure 2. Silicon dioxide (quartz), sodium aluminium silicate (albite), potassium, calcium, and $AlPO_4$ (berlinite) were matched to XRD spectrum of pumice. Amorph quartz structure of pumice was determined in the range of 20°-30° as expected [37-39]. Amorph quartz structure (20°-30°) was more pronounced in the mixed sample, which might be due to analytical limitations. Diffraction peak of zerovalent iron was observed at 44.9° (2 Theta) [40]. Also ferrous oxide was determined at 66.3° due to partial oxidation of nZVI surface as determined by Zhang et al. [40]. There were no impurities in commercial nZVI samples according to the XRD analysis. Albite, quartz, berlinite, potassium

and iron matched phases of mix materials. Amount of iron was determined as 8.4% of total peak area. The iron content (8.4%) obtained was similar to the amount added (10%).
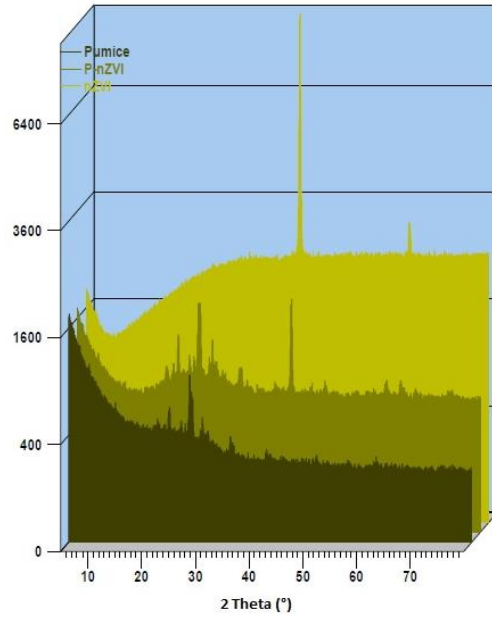
Figure 2. XRD graphs for used adsorbents (from dark green to light green: Pumice, P-nZVI, nZVI)

3.2. Removal of methylene blue

Treatment performances of bare pumice and mixed bed were evaluated using breakthrough curves of the effluent MB concentrations. The breakthrough curve of a specific adsorbate through a column in general depends on interparticle mass transfer, adsorption equilibrium and hydrodynamic conditions of the column. Therefore, operational parameters including flow rate (Q), initial MB concentration (C_0), bed height (H), and temperature (T) greatly affect breakthrough and dynamics of a column [24]. In this study, effects of initial MB concentration and adsorbent type on breakthrough time for methylene blue solution were investigated. Figure 3 shows the effect of initial MB concentrations in the range of 25 mg/L to 100 mg/L on breakthrough time for packed beds having bare pumice (a) and mixed pumice-nZVI (b).

At high initial concentrations for both adsorbent types, breakthrough was reached faster and slope of breakthrough curve was sharper. Effect of initial concentration on breakthrough point was observed when it decreased from 100 to 25 mg/L for each case. This might be related to sharper decrease in active sites of adsorbent at higher initial concentrations, which resulted in faster attainment of the breakthrough point [41]. As the C_0 increased methylene blue sorption rate increased. Subsequently, transfer of mass decreased, which resulted in decreasing of the length of adsorption zone. The MB removal rate of bare pumice was determined to be over 99% until 39th, 27th, 18th and

15th minutes for 25, 50, 75 and 100 ppm initial MB concentrations, respectively. However, MB removal rate of raw pumice decreased drastically, especially for 100 ppm and 75 ppm concentrations, which practically followed an identical trend. The change observed for 25 ppm curve (Figure 2a) was less drastic, drop from 99% to 20% adsorption happened within 27 minutes.
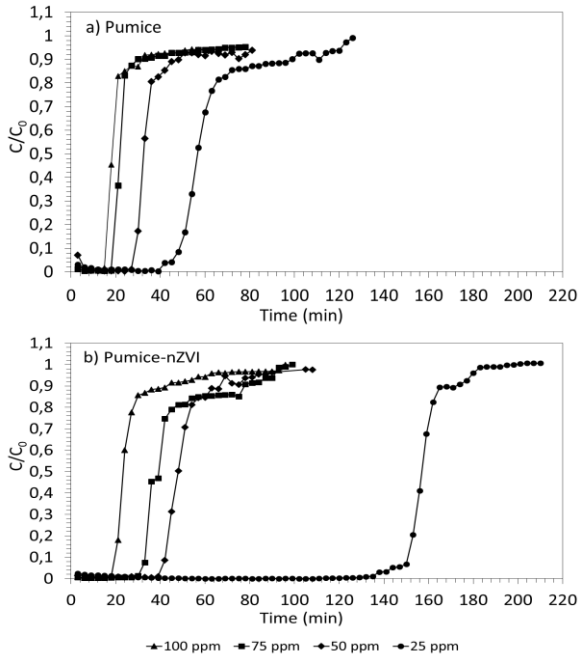
Figure 3. Breakthrough curves for bare pumice (a) and pumice-nZVI mix (b)

Mixing nZVI with pumice had a pronounced effect on the breakthrough curves (Figure 2b), being observed as a rightward shift on time scale. Especially the curve for 25 ppm has shifted significantly, more than tripling the time for achieving a treatment efficiency of 99%. Removal rate of mixed bed column reactor was over 99% at 132nd, 39th, 30th and 18th minutes for 25, 50, 75 and 100 ppm initial MB concentrations, respectively. Moreover, drops in treatment efficiencies as observed in breakthrough curves were not as drastic as their counterparts in pumice-only experiments. Determined MB removal rates have shown that nZVI supplement into the column filler has improved efficiency for 25 ppm C_0 significantly. There were also improvements observed for 50 ppm and 75 ppm experiments. However, the used pumice:nZVI ratio was clearly not having a significant effect on removal of 100 ppm MB. Removal phenomena of column reactor was determined better at low initial MB concentrations. This was due to decreasing of available sorbent area with increasing initial MB concentration. As the amount of adsorbed MB increased, decreasing sorption areas caused a decrease in concentration gradient between adsorbent and liquid phase. Several studies have been conducted for MB removal using different adsorbents from solutions. For instance, removal of MB using nZVI particles from water and water-ethanol aqueous solution with batch experiments

was investigated [41]. Adsorption capacities were calculated as 9.6 mg/g for water and 2.5 mg/g for water-ethanol mixture (50:50) at adsorbent dosage of 0.025 g nZVI and initial dye concentration of 10 mg/L.

3.3. Thomas model of MB removal kinetics

Breakthrough curve is theoretically determined by solving (often numerically) rigorous partial differential equations arising from the application of material balance and mass transfer equations for the bulk and adsorbed phases. However, several models are used extensively to simplify calculations. Thomas adsorption model [38] is one of the most widely applied models in column reactor performance studies. Table 1 compares the capacity and Thomas adsorption model parameter values obtained using both bare pumice and pumice-nZVI mixture at different initial concentrations.

Table 1. Thomas adsorption model outputs and adsorption capacities for both pumice and pumice-nZVI mixed bed

Adsorbent type	C_0 (mg/L)	K_T $\left(\dfrac{mL}{min\,mg}\right)$	$q_{e,exp}$ (mg/L)	$q_{e,theo}$ (mg/L)	SSE
Pumice	25	6.398	1.355	1.403	0.006
	50	2.447	1.927	1.891	0.074
	75	2.724	1.896	1.543	0.011
	100	1.865	2.798	2.597	0.111
Pumice-nZVI	25	6.287	1.706	1.638	0.022
	50	1.981	2.447	2.179	0.015
	75	2.468	2.349	2.019	0.01
	100	1.102	4.272	3.481	0.090

In this study, the Thomas adsorption model was utilized between saturation and breakthrough points in the column test using both pumice and pumice-nZVI mixed bed. For both adsorbent types, Thomas rate constant, K_T, tended to decrease and $q_{o,exp}$ increased when the initial concentration increased. In addition, experimental results were reproduced with high SSE values in the range of 0.006 to 0.111 as tabulated in Table 1. Correlation between experimental versus theoretical MB removal rates of pumice and pumice-nZVI were shown in Figure 4 and 5, respectively. Moderate positive correlation between experimental and modeling results have shown the predictive power of the model used. Predictive power of Thomas model was the best for 25 ppm initial MB concentration. With the increasing concentration, data got more scattered (Figures 4 and 5). Maximum adsorption capacities determined from the Thomas adsorption model (qe,theo., mg/g) were very close to experimental column capacities (qe,exp., mg/g). According to results, adsorption capacities of the adsorbents were determined as 2.8 (pumice) and 4.2 mg/g-adsorbent (pumice-nZVI), for initial MB concentration of 100 mg/L. Based on these results, we concluded that Thomas model suitably described adsorption of methylene blue by pumice and pumice-nZVI mixture in fixed bed column. An evaluation of maximum adsorption capacities reported in literature revealed comparability of our results (Table 2).

Table 2. Comparison of adsorption capacities of various adsorbents for the removal of MB

Adsorbent type	q_{max} (mg/g)	Operating conditions	References
Sand Graphite oxide-sand	0.07 0.74	flow rate: 2 mL/min, bed depth: 15 cm, initial MB concentration: 100 mg/L, pH: 4.21, operating time for sand adsorbent: 270 min, operating time for graphite oxide- sand adsorbent: 680 min	[43]
Cotton-alk	0.024	adsorbent dosage: 0.1 g, initial MB concentration: 250 mg/L, operating time: 10 min, stirring speed: 4000 rpm	[44]
Silica microspheres decorated with polydopamine nano-particles	14.68	flow rate: 5 mL/min, bed depth: 0.3 cm, adsorbent dosage: 0.37 g, initial MB concentration: 100 mg/L, pH: 3.0, operating time: 20 min	[45]
Biochar	4.97	flow rate: 1 L/h, bed depth: 0.32 m, adsorbent dosage: 400 g, initial MB concentration: 500 mg/L, pH: 7.0, temperature: 40 ºC	[46]
Microcrystalline Cellulose	1.44	adsorbent dosage: 5 g, initial MB concentration: 8 mg/L, pH: 6, temperature: 25 ºC, operating time: 3 min, stirring speed: 6000 rpm	[47]
Clay	6.3	adsorbent dosage: 0.1 g, initial MB concentration: 100 mg/L, temperature: 20 ºC, operating time: 1 h, stirring speed: 90 rpm	[48]
Pyrolyzed petrified sediment	2.39	adsorbent dosage: 0.5 g, initial MB concentration: 1x102- g/L, pH: 7, temperature: 30 ºC, operating time: 1 h, stirring speed: 90 rpm	[49]
Polyaniline nanotubes base/silica	10.3	adsorbent dosage: 0.05 g, initial MB concentration: 3.1 mg/L, temperature: 25 ºC, operating time: 60 min, stirring speed: 700 rpm	[50]
Mesoporous silica	5.58	flow rate: 2.68 mL/min, bed depth: 30 cm, adsorbent dosage: 0.1 g, initial MB concentration: 50 mg/L, pH: 2.0	[51]
Maize silk powder	7.8	adsorbent dosage: 80 mg, initial MB concentration: 20 mg/L	[52]
nZVI-bamboo	322.6	adsorbent dosage: 0.02 g, initial MB concentration: 140 mg/L, temperature: 25 ºC, operating time: 120 min, stirring speed: 165 rpm	[53]
iron-based nanoparticles	28.74	adsorbent dosage: 0.03 g, initial MB concentration: 140 mg/L	[54]
Zeolite	3.79	flow rate: 8.2 mL/min, bed depth: 30 cm, adsorbent dosage: 10 g, initial MB concentration: 50 mg/L, pH: 7.5, temperature: 25 ºC	[55]
Graphene oxide Titanate nanotube	21.7 16.1	adsorbent dosage: 0.1 g, pH: 6.8, operating time: 40 min, initial MB concentration: 10-60 mg/L, temperature: 25 ºC	[56]
Iron nanoparticles	2.5	adsorbent dosage: 0.025 g, initial MB concentration: 10mg/L, temperature: 25 ºC, water-ethanol mixture: 50-50	[57]
nanoscale zero-valent iron/ Zeolite Socony Mobil-5	3.76	adsorbent dosage: 0.5 g, pH: 2, stirring speed: 150 rpm, initial MB concentration: 20 mg/L, operating time: 90 min	[58]
Pumice Pumice-nZVI	2.80 4.27	flow rate: 2 mL/min, bed depth: 0.3 cm, adsorbent dosage: 0.08 g, initial MB concentration: 100 mg/L, temperature: 25 ºC	This study

4. Conclusion

Continuous mixed-bed column studies were performed to elucidate performances of selected adsorbents on removal of MB. nZVI is a high-on-demand adsorbent for its large specific surface area (~30-55 m²/g) and oxidation capacities for treatment of various pollutants. However, agglomeration and subsequent decrease of specific surface area are the issues in handling nZVI particles. Pumice, which is also used as an adsorbent, is a naturally found porous material with a low specific surface area (~2 m²/g). In order to produce an adsorbent medium that is cost-effective and resistant to agglomeration, we

supplemented pumice with nZVI particles. Experiments were conducted for pumice only and pumice-nZVI mix adsorbents. Laboratory-scale column studies demonstrated that MB removal efficiencies increased with increasing of binding sites of column bed. However; removal performance was greatly influenced by the initial dye concentration for bare pumice and nZVI-pumice fixed bed columns. Also, adsorption capacity of adsorbents increased with increasing initial MB concentrations whereas, breakthrough time decreased on increasing concentrations. Application of Thomas adsorption model demonstrated that it was successful in

capturing the experimental removal efficiencies in fixed column beds.
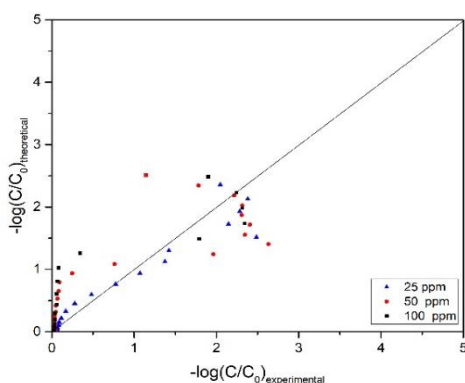
Figure 4. Distribution of experimental and theoretical MB removal of pumice
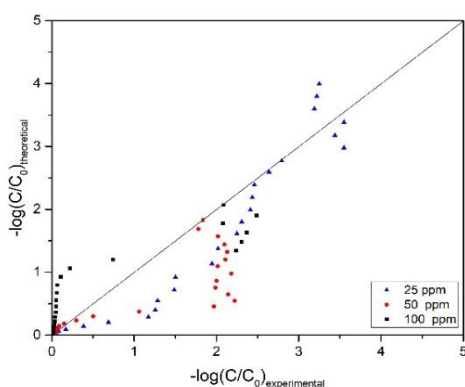
Figure 5. Distribution of experimental and theoretical MB removal of pumice-nZVI

Acknowledgement

References

[1]   Paździor, K., Wrębiak, J., Klepacz-Smółka, A., Gmurek, M., Bilińska, L., Kos, L., Sójka-Ledakowicz, J., Ledakowicz, S. 2017. Influence of ozonation and biodegradation on toxicity of industrial textile wastewater. Journal of Environmental Management, 195(Pt 2), 166–173.

[2]   Holkar, C. R., Jadhav, A. J., Pinjari, D. V., Mahamuni, N. M., Pandit, A. B. 2016. A critical review on textile wastewater treatments: possible approaches. Journal of Environmental Management, 182, 351–366.

[3]   Manna, S., Roy, D., Saha, P., Gopakumar, D., Thomas, S. 2017. Rapid methylene blue adsorption using modified lignocellulosic materials. Process Safety and Environmental Protection, 107, 346–356.

[4]   Nassar, N. N. 2010. Kinetics, mechanistic, equilibrium, and thermodynamic studies on the adsorption of acid red dye from wastewater by γ-Fe2O3 nanoadsorbents. Seperation Science and Technology, 45(8), 1092–1103.

[5]   Li, Y., Sun, J., Du, Q., Zhang, L., Yang, X., Wu, S., Xia ,Y., Wang, Z., Xia, L., Cao A. 2014. Mechanical and dye adsorption properties of graphene oxide/chitosan composite fibers prepared by wet spinning. Carbohydrate Polymers, 102, 755–761.

[6]   Abbasi, A. R., Karimi, M., Daasbjerg, K. 2017. Efficient removal of crystal violet and methylene blue from wastewater by ultrasound nanoparticles Cu-MOF in comparison with mechanosynthesis method. Ultrasonics Sonochemistry, 37, 182–191.

[7]   Chinoune, K., Bentaleb, K., Bouberka, Z., Nadim, A., Maschke, U. 2016. Adsorption of reactive dyes from aqueous solution by dirty bentonite. Applied Clay Science, 123, 64–75.

[8]   Zhang, S., Li, H., Yang, Z. 2017. Controllable synthesis of WO3 with different crystalline phases and its applications on methylene blue removal from aqueous solution. Journal of Alloys Compounds, 722, 555–563.

[9]   Chen, J., Feng, J., Yan, W. 2016. Influence of metal oxides on the adsorption characteristics of PPy/metal oxides for Methylene Blue. Journal of Colloid Interface Science, 475, 26–35.

[10] Neamtu, M., Yediler, A., Siminiceanu, I., Macoveanu, M., Kettrup, A. 2004. Decolorization of disperse red 354 azo dye in water by several oxidation processes—a comparative study. Dyes and Pigments, 60(1), 61–68.

[11] Mohammed, G. R., Zewail, T. M., El-Tawail, Y. A. 2014. Investigation of color removal from methylene blue containing solutions by electrocoagulation/flotation in a batch-agitated electrochemical reactor. Environmental Progress and Sustainable Energy, 33(2), 369–377.

[12] Lau, Y. Y., Wong, Y. S., Teng, T. T., Morad, N., Rafatullah, M., Ong, S. A. 2015. Degradation of cationic and anionic dyes in coagulation–flocculation process using bi-functionalized silica hybrid with aluminum-ferric as auxiliary agent. RSC Advances, 5(43), 34206–34215.

[13] Huang, J., Peng, L., Zeng, G., Li, X., Zhao, Y., Liu, L., Li, F., Chai, Q. 2014. Evaluation of micellar enhanced ultrafiltration for removing methylene blue and cadmium ion simultaneously with mixed surfactants. Seperation and Purification Technology, 125(7 April 2014), 83–89.

[14] Robinson, T., Chandran, B., Nigam, P. 2002. Effect of pretreatments of three waste residues,

wheat straw, corncobs and barley husks on dye adsorption. Bioresource Technology, 85(2), 119–124.

[15] Dil, E. A., Ghaedi, M., Asfaram, A. 2017. The performance of nanorods material as adsorbent for removal of azo dyes and heavy metal ions: application of ultrasound wave, optimization and modeling. Ultrasonics Sonochemistry, 34, 792–802.

[16] Ali, I., Asim, M., Khan, T. A. 2012. Low cost adsorbents for the removal of organic pollutants from wastewater. Journal of Environmental Management, 113, 170–183.

[17] Crini, G. 2006. Non-conventional low-cost adsorbents for dye removal: a review. Bioresource Technology, 97(9), 1061–1085.

[18] Gupta, V. K. 2009. Application of low-cost adsorbents for dye removal–a review. Journal of Environmental Management, 90, 2313–2342.

[19] Zhang, J., Zhou, Y., Jiang, M., Li, J., Sheng, J. 2015. Removal of methylene blue from aqueous solution by adsorption on pyrophyllite. Journal of Molecular Liquids, 209, 267–271.

[20] Popa, N., Visa, M. 2017. The synthesis, activation and characterization of charcoal powder for the removal of methylene blue and cadmium from wastewater. Advanced Powder Technology, 28(8), 1866–1876.

[21] Dasgupta, J., Sikder, J., Chakraborty, S., Curcio, S., Drioli, E. 2015. Remediation of textile effluents by membrane based treatment techniques: A state of the art review. Journal of Environmental Management, 147, 55–72.

[22] Bayramoglu, M., Kobya, M., Can, O. T., Sozbir, M. 2004. Operating cost analysis of electroagulation of textile dye wastewater. Seperation and Purification Technology, 37(2), 117–125.

[23] Nawaz, M. S., Ahsan, M. 2014. Comparison of physico-chemical, advanced oxidation and biological techniques for the textile wastewater treatment. Alexandria Engineering Journal, 53(3), 717–722.

[24] Harman, B. I., Genisoglu, M. 2016. Synthesis and Characterization of Pumice-Supported nZVI for Removal of Copper from Waters. Advanced Material Science Engineering, 2016 (2016), 1-10.

[25] Han, R., Wang, Y., Zhao, X., Wang, Y., Xie, F., Cheng, J., Tang, M. 2009. Adsorption of methylene blue by phoenix tree leaf powder in a fixed-bed column: experiments and prediction of breakthrough curves. Desalination, 245(1-3), 284–297.

[26] Liu, T., Wang, Z. L., Yan, X., Zhang, B. 2014. Removal of mercury (II) and chromium (VI) from wastewater using a new and effective composites: Pumice-supported nanoscale zero-valent iron. Chemical Engineering, 245, 34-40.

[27] Stefaniuk, M., Oleszczuk, P., Ok, Y. S. 2016. Review on nano zerovalent iron (nZVI): From synthesis to environmental applications. Chemical Engineering Journal, 287, 618-632.

[28] Liu, T., Yang, Y., Wang, Z.L., Sun, Y. 2016. Remediation of arsenic (III) from aqueous solutions using improved nanoscale zero-valent iron on pumice. Chemical Engineering Journal, 288, 739-744.

[29] Kim, S. H., Kamala-Kannan, S., Lee, K.J., Park, Y.J., Shea P.J., Lee, W.H., Kim, H. M., Ok, B.T. 2013. Removal of Pb(II) from aqueous solution by a zeolite nanoscale zero valent iron composite. Chemical Engineering Journal, 217, 54-60.

[30] Ezzatahmadi, N., Ayoko, G.A., Miller, G.J., Speight, R., Yan, C., Li, J., Li, S., Xi, Y. 2017. Clay-supported nanoscale zero-valent iron composite materials for the remediation of contaminated aqueous solutions: A review. Chemical Engineering Journal, 312, 336-350.

[31] Harman, B.I. and Ibrahim, N.S. 2018. Competitive Adsorption of Heavy Metals from Water Using Pumice Supported Nanoscale Zero-Valent Iron. Special Issue of the 7th International Advances in Applied Physics and Materials Science (APMAS 2017), 134, 171-173.

[32] Samarghandi, M.R., Zarrabi, M., Amrane, A., Soori, M.M., Sepehr, M.N. 2013. Removal of Acid Black Dye by Pumice Stone as a low cost adsorbent; kinetic, thermodynamic and equilibrium studies. Environmental Engineering and Management Journal, 12(11)2137-2147.

[33] Liu, T., Wang, Z. L., Sun, Y. 2015. Manipulating the morphology of nanoscale zero-valent iron on pumice for removal of heavy metals from wastewater. Chemical Engineering Journal, 263, 55–61.

[34] Cifci, D.I., Meric, S. 2016. Optimization of Methylene Blue adsorption by pumice powder. Advances in Environmental Research, 5, 37-50.

[35] İpek, İ. Y., Kabay, N., Yüksel, M. 2013. Modeling of fixed bed column studies for removal of boron from geothermal water by selective chelating ion exchange resins. Desalination, 310, 151–157.

[36] Recepoğlu, Y. K., Kabay, N., Ipek, I. Y., Arda, M., Yüksel, M., Yoshizuka, K., Nishihama, S. 2018. Packed bed column dynamic study for boron removal from geothermal brine by a chelating fiber and breakthrough curve analysis by using mathematical models. Desalination, 437, 1–6.

[37] Arrigo, I., Catalfamo, P., Cavallari, L., Dipasquale, S., 2007. Use of zeolitized pumice waste as a water softening agent. Journal of Hazardous Materials, 147, 513–517.

[38] Chuan, X.Y., Hirano, M., Inagaki, M., 2004. Preparation and photocatalytic performance of anatase-mounted natural porous silica, pumice, by hydrolysis under hydrothermal conditions. Applied Catalysis B: Environmental, 51(4), 255-260.

[39] Ersoy, B., Sariisik, A., Dikmen, S., Sariisik, G., 2010. Characterization of acidic pumice and determination of its electrokinetic properties in water. Powder Technology, 197(1-2), pp.129-135.

[40] Zhang, X., Lin, S., Chen, Z., Megharaj, M., Naidu, R., 2011. Kaolinite-supported nanoscale zero-valent iron for removal of Pb2+ from aqueous solution: reactivity, characterization and mechanism. Water Research, 45, 3481-3488.

[41] Sawafta, R., Shahwan, T. 2019. A comparative study of the removal of methylene blue by iron nanoparticles from water and water-ethanol solutions. Journal of Molecular Liquids, 273, 274–281.

[42] Thomas, H. C. 1944. Heterogeneous Ion Exchange in a Flowing System. Journal of the American Chemical Society, 66(10), 1664–1666.

[43] Gong, J. L., Zhang, Y. L., Jiang, Y., Zeng, G. M., Cui, Z. H., Liu, K., Deng, C. H., Niu, Q. Y., Deng, J. H., Huan, S. Y. 2015. Continuous adsorption of Pb(II) and methylene blue by engineered graphite oxide coated sand in fixed-bed column. Applied Surface Science, 330, 148–157.

[44] Ding, Z., Hu, X., Zimmerman, A. R., Gao, B. 2014. Sorption and cosorption of lead (II) and methylene blue on chemically modified biomass. Bioresource Technology, 167, 569–573.

[45] Germi, T. A., Nematollahzadeh, A. 2016. Bimodal porous silica microspheres decorated with polydopamine nano-particles for the adsorption of methylene blue in fixed-bed columns. Journal of Colloid and Interface Science, 470, 172–182.

[46] Bharti, V., Vikrant, K., Goswami, M., Tiwari, H., Sonwani, R.K., Lee, J., Tsang, D.C., Kim, K.H., Saeed, M., Kumar, S., Rai, B.N., 2019. Biodegradation of methylene blue dye in a batch and continuous mode using biochar as packing media. Environmental research, 171, 356-364.

[47] Tan, K. B., Abdullah, A. Z., Horri, B. A., Salamatinia, B. 2016. Adsorption mechanism of microcrystalline cellulose as green adsorbent for the removal of cationic methylene blue dye. Chemical Society of Pakistan, 38, 651-664.

[48] Gürses, A., Karaca, S., Doğar, Ç., Bayrak, R., Açıkyıldız, M., Yalçın, M. 2004. Determination of adsorptive properties of clay/water system: methylene blue sorption. Journal of Colloid and Interface Science, 269 (2), 310–314.

[49] Aroguz, A. Z., Gulen, J., Evers, R. H., 2008. Adsorption of methylene blue from aqueous solution on pyrolyzed petrified sediment. Bioresource, 99 (6), 1503-1508.

[50] Ayad, M. M., El-Nasr, A. A., Stejskal, J. 2012. Kinetics and isotherm studies of methylene blue adsorption onto polyaniline nanotubes base/silica composite. Journal of Industrial and Engineering Chemistry, 18 (6), 1964-1969.

[51] Sheng, L., Zhang, Y., Tang, F., Liu, S. 2018. Mesoporous/microporous silica materials: Preparation from natural sands and highly efficient fixed-bed adsorption of methylene blue in wastewater. Microporous and Mesoporous Materials, 257, 9-18.

[52] Miraboutalebi, S. M., Nikouzad, S. K., Peydayesh, M., Allahgholi, N., Vafajoo, L., McKay, G. 2017. Methylene blue adsorption via maize silk powder: Kinetic, equilibrium, thermodynamic studies and residual error analysis. Process Safety and Environmental Protection, 106, 191-202.

[53] Shaibu, S. E., Adekola, F. A., Adegoke, H. I., Ayanda, O. S. 2014. A Comparative Study of the Adsorption of Methylene Blue onto Synthesized Nanoscale Zero-Valent Iron-Bamboo and Manganese-Bamboo Composites. Materials, 7 (6), 4493-4507.

[54] Lin, J., Weng, X., Jin, X., Megharaj, M., Naidu, R., Chen, Z. 2015. Reactivity of iron-based nanoparticles by green synthesis under 3 various atmospheres and their removal mechanism of methylene blue. Royal Society of Chemistry, 5, 70874-70882.

[55] Han, R., Wang, Y., Zou, W., Wang, Y., Shi, J. 2007. Comparison of linear and nonlinear analysis in estimating the Thomas model parameters for methylene blue adsorption onto natural zeolite in fixed-bed column. Journal of Hazardous Materials, 145 (1-2), 331–335.

[56] Sawafta, R., Shahwan, T. 2019. A Comparative Study of the Removal of Methylene Blue by Iron Nanoparticles from Water and Water-Ethanol Solutions. Journal of Molecular Liquids, 273, 274-281.

[57] Nguyena, C. H., Juang, R. S. 2019. Efficient removal of methylene blue dye by a hybrid adsorption– photocatalysis process using reduced graphene oxide/titanate nanotube composites for water reuse. Journal of Industrial and Engineering Chemistry, 76, 296–309.

[58] Hammed, A. K., Dewayanto, N., Du, D., Rahim, M. H. A., Nordin, M. R. 2016. Novel modified ZSM-5 as an efficient adsorbent for methylene blue removal. Journal of Environmental Chemical Engineering, 4 (3), 2607-2616.